Large RKKY coupling from multiple scattering in armchair graphene nanoribbons

Van Minh Nguyen and C. S. Chu*
Department of Electrophysics, National Chiao Tung University, Hsinchu 30010, Taiwan

(Received 14 February 2020; revised manuscript received 26 April 2020; accepted 29 April 2020; published 12 May 2020)

We consider the Ruderman-Kittel-Kasuya-Yosida (RKKY) type coupling between two magnetic impurities on metallic armchair graphene nanoribbons (AGNR). Our key findings are that the lowest-order RKKY (LO-RKKY) coupling does not describe the coupling physics, and a full implementation of electron multiple scattering in RKKY coupling leads to orders of magnitude enhancement in the coupling magnitude. Key physics of our findings are revealed in our analysis of the LO-RKKY coupling. Within the Born approximation for the electron-magnetic-impurity scattering, the LO-RKKY coupling has inherited the singular density of states feature so that incident electrons at AGNR-subband band edges give finite contributions. Our other finding, that contribution from a gapped subband to LO-RKKY coupling is very small, implies then that severe cancellations must have occurred between states at its subband band edges and states not at its subband band edges. Magnitudes of the cancellation terms are each of the same order as the LO-RKKY coupling. This cancellation no longer occurs when full multiple scattering is reinstated. Contributions to the RKKY coupling from states at subband band edges are entirely suppressed, due to the restoring of the finiteness in the wave functions of these states. Contributions from states not from the subband band edges, though modified, retain their orders of magnitude. Analytic expressions have been obtained to further illustrate the physics.

DOI: 10.1103/PhysRevB.101.195419

I. INTRODUCTION

Magnetic impurities embedded in metal can interact via an important indirect exchange coupling, the Ruderman-Kittel-Kasuya-Yosida (RKKY) coupling [1–3], where conduction-electron spins mediate between the impurities. RKKY interaction has been studied in rare-earth metals [4], metal surfaces [5], magnetic metallic multilayers [6], dilute magnetic semiconductors [7], one- or two-dimensional semiconductors with Rashba spin-orbit coupling [8], and carbon nanotubes [9]. The successful fabrication of graphene [10,11] has prompted RKKY interaction studies on graphene sheets [12–26], bilayer graphene [27–29], and in graphene nanoribbons [30–35]. Most recently, the trending new field of topological physics has spawned RKKY interaction studies in monolayer MoS_2 [36], in zigzag silicene nanoribbons [37], in transition metal dichalcogenides [38], and in three-dimensional Dirac semimetals [39].

Research in the RKKY coupling $J_{\rm eff}$ in graphene sheet has kept up to the second order in J [12–26], the exchange coupling between a magnetic impurity and the mediating electrons. As such it is the lowest-order RKKY (LO-RKKY) coupling $J_{\rm eff}^{(1)}$ that they have obtained. Multiple scattering of the electrons between the magnetic-impurity pair is justifiably reckoned negligible. Issues of interests include the dependence of the $J_{\rm eff}^{(1)}$ on the spatial separation between the two magnetic impurities, the difference in the coupling characteristics for two magnetic impurities that are of the same or different *sublattice-site* type, and possible resonant enhancement of the LO-RKKY coupling from introducing an onsite potential from the magnetic impurity to the electrons [25]. The electronic nature of the RKKY coupling motivates research efforts to explore ways to either enhance the magnitude of the coupling [25] or to monitor the sign of the coupling [23].

Research in the RKKY coupling in graphene nanoribbons focuses also on the calculation of $J_{\rm eff}^{(1)}$ [16,30,32–35,40]. An earliest study on the RKKY in graphene nanoribbon focused on the zigzag graphene nanoribbons while commenting that the armchair edge did not significantly affect the RKKY [16]. Invoking an effective Hamiltonian for the armchair graphene nanoribbons (AGNR), which is valid near the zero energy, analytic expression for $J_{\rm eff}^{(1)}$ was obtained [30], showing ferromagnetic (antiferromagnetic) coupling when the two magnetic impurities are of the same (different) *sublattice-site* type, and that $J_{\rm eff}^{(1)}$ varies as L^{-1}, where L is the longitudinal separation between the two magnetic impurities. This same L dependence in $J_{\rm eff}^{(1)}$ was also obtained numerically [40], while its sensitivity to the transverse locations of the magnetic impurities was shown [40]. The issue of going beyond the LO-RKKY was addressed by invoking a super-unit-cell approach [31], where instead of a magnetic-impurity pair in the AGNR, super unit cells each containing two magnetic impurities are considered. The problem was solved by the method of diagonalization [31]. Even though the multiple scattering feature between the two magnetic impurities in a super unit cell has been incorporated, other multiple scatterings such as between magnetic impurities from different super unit cells have also been included. Concern about using such a super-unit-cell approach for even a single magnetic impurity had been raised [15]. Furthermore, two spin-aligned magnetic impurities in

*cschu@cc.nctu.edu.tw

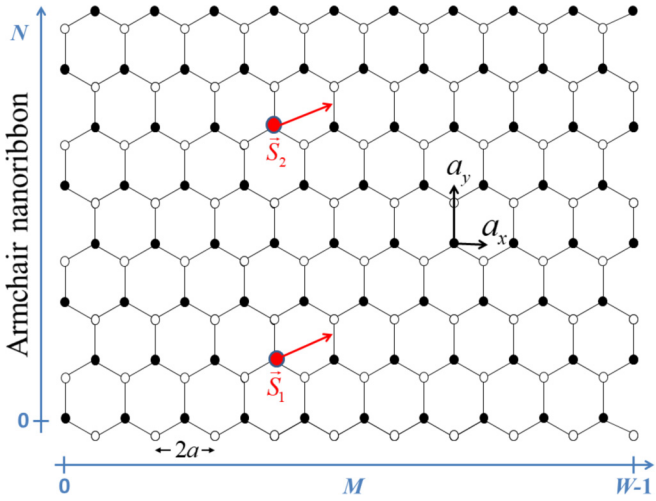

FIG. 1. Schematic illustration of an armchair graphene nanoribbon with $W = 20$ carbon chains. Two magnetic impurities occupying the A-type carbon sites are shown. The lengths labeled by a_x and a_y are a and $\sqrt{3}a$, respectively.

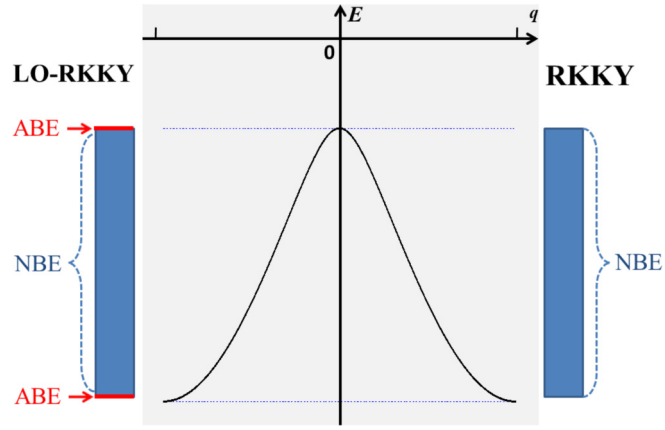

FIG. 2. Conceptual highlight of our key findings. Contributions to LO-RKKY coupling from a gapped subband (as shown) suffers severe cancellation between its states from *at-the-band-edge* (ABE) and from the *non-band-edge* (NBE) regions. Full multiple scattering in RKKY suppresses the ABE terms, leading to much enhanced RKKY coupling.

a super-unit-cell arrangement would cause the chemical potential to become spin dependent. These added features could lead to nontrivial effects not present to the original problem of a magnetic-impurity pair. It is then of great interest to consider the RKKY coupling for a magnetic-impurity pair on graphene nanoribbons and treat in full the multiple scattering of the mediating electrons between the impurities. We therefore opt, in this work, to calculate $J_{\rm eff}$ for a magnetic-impurity pair on AGNRs, as is shown in Fig. 1, that are connected at their two ends to reservoirs of the same chemical potential.

Multiple scattering is known to be crucial in quantum transport in quasi-one-dimensional system [41], leading to transmission dip structures at energies just below, and very close to, subband band edges for the case of attractive scatterers. It is associated with the singular density of states at subband band edges, and the formation of quasibound states at the subband band edges for attractive scatterers [42].

In this work, multiple scattering is found to drastically enhance the magnitude of the RKKY coupling $J_{\rm eff}$. It is shown, for instance, greater than $J^{(1)}_{\rm eff}$, the LO-RKKY results, by up to two orders of magnitude for an AGNR of width $W = 20$. We show that understanding of this drastic enhancement of $J_{\rm eff}$ is hidden in $J^{(1)}_{\rm eff}$, and particularly, in the way that $J^{(1)}_{\rm eff}$ ends up in a very small magnitude. Contributions to $J^{(1)}_{\rm eff}$ are solely from the gapless subband while those from the gapped subbands are very small. Meanwhile, the Born approximation treatment of the electron-magnetic-impurity scattering has carried with it the singular density of state features (at subband band edges) so that there are finite contributions to $J^{(1)}_{\rm eff}$ from incident states at the subband band edges. So, our other findings that the very small contribution from a gapped subband to $J^{(1)}_{\rm eff}$ must be a result of a large cancellation among incident states from the same gapped subband. More specifically, the cancellation must have occurred between contributions from *at-the-band-edge* states and contributions from *non-band-edge* states, all from the same gapped subband. We also find that magnitudes of these two cancellation terms are each of the same order as the $J^{(1)}_{\rm eff}$. On the other hand, the large difference in the range of energy, from which the at-the-band-edge and the non-band-edge terms collect their contributions, strongly hints that the two terms could be affected differently should other factor, such as multiple scattering, be included in our calculations. Indeed, we find out that when multiple scattering is fully incorporated to the electrons, the two terms are affected differently. The at-the-band-edge term is suppressed because the scattering wave functions are no longer singular at the band edges. The non-band-edge term remains essentially in the same order of magnitude. This opens up significant contribution to $J_{\rm eff}$ from gapped subbands, leading to the drastic enhancement in the magnitude of $J_{\rm eff}$. A conceptual highlight of the aforesaid reason for the dramatic enhancement in $J_{\rm eff}$ over that in $J^{(1)}_{\rm eff}$ is presented in Fig. 2.

This paper is organized as follows. In Sec. II, we present our theoretical framework and apply it to obtain our LO-RKKY coupling $J^{(1)}_{\rm eff}$ results, up to J^2, both analytical and numerical. This section also serves to establish the notations we use in this work. In Sec. III, we present the RKKY coupling $J_{\rm eff}$ for the case when full multiple scattering of the mediating electrons between the magnetic impurities is implemented. Our results, both analytic and numerical, that $J_{\rm eff}$ is greater than $J^{(1)}_{\rm eff}$ by up to two orders of magnitude will be presented in this section. Finally, we present our conclusion in Sec. IV.

II. RKKY COUPLING: LOWEST ORDER

This section first presents our theoretical framework for the RKKY coupling between two magnetic impurities on AGNRs. We then focus on the lowest-order RKKY (LO-RKKY) coupling, in which the mediating electrons are treated within the Born approximation. This LO-RKKY result turns out to be important for this work because it provides a basis and a guide for a clearer presentation of our RKKY coupling calculation in the next section, where full multiple scattering is treated for the mediating electrons. It is also noted that the LO-RKKY

coupling consideration has been the main approach taken up for the RKKY research so far. Thus, to our LO-RKKY results, we have performed extensive analytical analysis in order to obtain an unambiguous picture for the next section. Toward that end, and to concentrate on the physics behind our findings, we opt to focus upon the case when the two magnetic impurities have their spin oriented perpendicular to the plane of the AGNRs, namely, $\mathbf{S} = S_z\hat{z}$. Our results for the RKKY coupling should remain the same had we considered $\mathbf{S}$ of general orientations because the pristine AGNR do not have spin-dependent interaction. This section also serves to establish the notations that we have adopted in this work.

The calculation of the RKKY coupling is by way of a density matrix approach, with the density matrix ρ defined by

$$\rho = \sum_{\gamma,\mathbf{k}_n\nu} f(\gamma\varepsilon(\mathbf{k}_n))\,|\Psi_{\mathbf{k}_n\nu}\rangle\langle\Psi_{\mathbf{k}_n\nu}|, \tag{1}$$

where $f(E)$ is the Fermi-Dirac distribution for the reservoirs at the two ends of the AGNR, both having the same chemical potential μ, and γ denotes the sign of the incident state energy $E(\mathbf{k}_n,\gamma) = \gamma\varepsilon(\mathbf{k}_n)$ where the incident state $|\psi_{\mathbf{k}_n}\rangle$ is given in Eq. (A4), and γ is kept implicit in $|\psi_{\mathbf{k}_n}\rangle$. Associated basic parameters for AGNRs are defined in the paragraph in which Eq. (A4) is contained. The corresponding scattered state $|\Psi_{\mathbf{k}_n\nu}\rangle$, in the presence of the two magnetic impurities located at AGNR lattice sites $|\mathcal{I}\rangle = |\mathbf{R}_\mathcal{I}, s_\mathcal{I}\rangle$, for $\mathcal{I} \in 1, 2$, and described by an exchange model

$$\hat{V} = J\sum_{\mathcal{I}} |\mathcal{I}\rangle\langle\mathcal{I}|\ \mathbf{S}_\mathcal{I}\cdot\sigma, \tag{2}$$

is given, in the lattice representation of the Lippmann-Schwinger equation, by

$$\Psi_{\mathbf{k}_n\nu,\nu}(\mathcal{J}) = \psi_{\mathbf{k}_n}(\mathcal{J}) + J\sum_{\mathcal{I}} G_{\mathcal{J}\mathcal{I}}(\gamma\varepsilon(\mathbf{k}_n))S_\mathcal{I}\,\nu\Psi_{\mathbf{k}_n\nu,\nu}(\mathcal{I}). \tag{3}$$

Here, $|\mathcal{J}\rangle$ denotes a general AGNR lattice site, J is the exchange coupling constant (in units of t_0 the graphene hopping constant), $S_\mathcal{I}$ is of unity magnitude, in units of $\hbar$, σ is the Pauli vector for the electron spin, with $\sigma_z|\nu\rangle = \nu|\nu\rangle$, and $G_{\mathcal{J}\mathcal{J}'}$ is given in Eq. (A1). The scattered state $|\Psi_{\mathbf{k}_n\nu}\rangle = |\Psi_{\mathbf{k}_n\nu,\nu}\rangle\,|\nu\rangle$ conserves spin when $\mathbf{S}_\mathcal{I}$ is along $\hat{z}$. The average $\langle V\rangle$, defined by $\langle V\rangle = \mathrm{Tr}[\rho\hat{V}]$, depends on the relative orientations of $S_\mathcal{I}$'s, and is obtained to be

$$\langle V\rangle = J\sum_{\mathbf{k}_n,\nu}\sum_{\mathcal{I}} f(-\varepsilon(\mathbf{k}_n))|\Psi_{\mathbf{k}_n\nu,\nu}(\mathcal{I})|^2\nu S_\mathcal{I}. \tag{4}$$

In Eq. (4), we have set $\mu = 0$.

The LO-RKKY coupling result is obtained from Eq. (4) by replacing $\Psi_{\mathbf{k}_n\nu,\nu}(\mathcal{I})$ on the right-hand side of Eq. (3) by $\psi_{\mathbf{k}_n}(\mathcal{I})$. This gives us the lowest order $\langle V\rangle^{(1)}$:

$$\frac{\langle V\rangle^{(1)}}{J^2} = 2\sum_{\mathbf{k}_n,\nu}\sum_{\mathcal{I},\mathcal{I}'}\mathrm{Re}\big[G_{\mathcal{I}\mathcal{I}'}(-\varepsilon_{\mathbf{k}_n})\psi_{\mathbf{k}_n}(\mathcal{I})\psi^*_{\mathbf{k}_n}(\mathcal{I}')\big]S_\mathcal{I}S_{\mathcal{I}'}. \tag{5}$$

Here, $\varepsilon(\mathbf{k}_n) = \varepsilon_{\mathbf{k}_n}$ is by our definition positive. Separating Eq. (5) into S_1S_2-independent and S_1S_2-dependent terms gives $\langle V\rangle^{(1)} = V_0^{(1)} + V_1^{(1)}$. The S_1S_2-dependent term $V_1^{(1)}$ is related to the LO-RKKY coupling, and can be simplified using the symmetry property $G_{\mathcal{J}\mathcal{J}'}(E) = G_{\mathcal{J}'\mathcal{J}}(E)$, in Eq. (A5), to give

$$V_1^{(1)} = \frac{4J^2}{\pi}S_1S_2\sum_n\varphi_n(1,2)\int_{-\pi}^{\pi}dq\,\mathrm{Re}\big[G_{12}(-\varepsilon_{\mathbf{k}_n})\big] \times \mathrm{Re}[C^{s_1}(\mathbf{k}_n,-1)C^{s_2*}(\mathbf{k}_n,-1)e^{iqL_{12}}]. \tag{6}$$

Here, $\varphi_n(1,2)$ is defined in Eq. (A3), $C^s(\mathbf{k}_n,\gamma)$ are pseudospin coefficients for $(s \in \mathrm{A/B})$ site types, defined in Eq. (A4), and L_{12} is the longitudinal separation between the two magnetic impurities, in units of $\sqrt{3}a$.

Equation (6) suggests the form $V_1^{(1)} = J_{\mathrm{eff}}^{(1)}S_1S_2$, where $J_{\mathrm{eff}}^{(1)}$ is the lowest-order RKKY coupling constant. In the following, we will evaluate $J_{\mathrm{eff}}^{(1)}$ for the cases of *same-site* and *different-site* types.

A. Same-site type $J_{\mathrm{eff}}^{(1)}$

When the two magnetic impurities are located on the same site type, we have $s_1 = s_2$, and $|C^s(\mathbf{k}_n,\gamma)|^2 = \frac{1}{2}$, such that the integrand becomes an even function of q, and the expression of $J_{\mathrm{eff}}^{(1)}$ is further simplified to

$$J_{\mathrm{eff}}^{(1)} = \frac{2J^2}{\pi^2}\sum_{n,n'}\varphi_n(1,2)\,\varphi_{n'}(1,2)\,I_{nn'}, \tag{7}$$

where

$$I_{nn'} = \int_0^\pi dq\,\mathrm{Re}\big[g^{12}_{n'}(-\varepsilon_{\mathbf{k}_n})\big]\cos(qL). \tag{8}$$

We stress that $g^{12}_{n'}(-\varepsilon_{\mathbf{k}_n})$, defined in Eq. (A2), has its analytical expressions given by Eq. (A8), in the non-band-edge regime, and by Eqs. (A9) and (A10), in the at-the-band-edge regime. These two regimes will be important for our analysis in the following. Here, $L = |L_{12}|$.

We will evaluate $J_{\mathrm{eff}}^{(1)}$ both numerically and analytically. Our analytic calculation will focus on the integral I_{nn}, and our numerical evaluation will use an alternate form, to be shown below, that is derived from Eq. (7). From this alternate form of $J_{\mathrm{eff}}^{(1)}$ we will see that contribution from $I_{nn'}$, except for $n = n' = n_0$, is very small, and this is also confirmed in our numerical calculation. Here, the n_0 subband denotes the gapless subband. To arrive at the alternate form for $J_{\mathrm{eff}}^{(1)}$, we start from the same-site-type form of $g^{12}_{n'}(-\varepsilon_{\mathbf{k}_n})$ in Eq. (A2) to get

$$g^{12}_{n'}(-\varepsilon_{\mathbf{k}_n}) = \int_0^\pi dq'\cos(q'L) \times\left[\frac{1}{-\varepsilon_{\mathbf{k}_n}-\varepsilon_{\mathbf{k}'_{n'}}+i\eta} + \frac{1}{-\varepsilon_{\mathbf{k}_n}+\varepsilon_{\mathbf{k}'_{n'}}+i\eta}\right]. \tag{9}$$

Recalling that $\varepsilon_{\mathbf{k}_n}$ is positive, the second term in Eq. (9) has pole features in its integrand. Now, by substituting Eq. (9) to Eqs. (8) and (7) and following by interchanging of indices $n \leftrightarrow n'$ and integration variables $q \leftrightarrow q'$, we can show that terms that carry the pole features are zero. As a result, we have

$$I^{(1)}_{nn'} = -\int_0^\pi\int_0^\pi dq\,dq'\,\frac{\cos(qL)\cos(q'L)}{\varepsilon_{\mathbf{k}_n}+\varepsilon_{\mathbf{k}'_{n'}}}, \tag{10}$$

where η in the denominator can be dropped.

This form of $I_{nn'}$ clearly shows that there is no singular feature in the integrand, making the numerical calculation straightforward. Furthermore, the denominator of the integrand contains cos$q$ and cosq' while the numerator contains cos(qL) and cos$(q'L)$, so it is understandable that for, say, $L > 10$, we expect to see great cancellations in the integral so that $I_{nn'}$ becomes very small. This argument fails for the case when $n = n' = n_0$, where n_0 is the gapless subband such that $\varepsilon_{\mathbf{k}_{n_0}} = 0$ at $q = 0$. Hence, the most significant contribution to $I_{n_0 n_0}$ will come from the linear dispersion region of $\varepsilon_{\mathbf{k}_{n_0}}$. On the other hand, very close to the integration region $q \sim 0$ and $q' \sim 0$, the integral does not give a finite contribution because it is a two-dimensional integral. In short, Eq. (10) leads us to the expectation that the sole contribution to $J^{(1)}_{\rm eff}$ should be from the $I_{n_0 n_0}$ integral. This is confirmed by our numerical results.

Equipped with these insights, we focus our analytical calculation on the $n = n' \neq n_0$ case, but turn to Eq. (8) for our calculation. The motivation is to see how this I_{nn} integral ends up in a very small value. Our aim here is to obtain, from Eq. (8), the two cancellation terms that upon their severe cancellations give a very small I_{nn}. The form of I_{nn} warrants [according to the discussion following Eq. (A8)] the splitting of the integral into the at-the-band-edge and non-band-edge terms.

On the other hand, the $n \neq n'$ cases of Eq. (8) present no need for similar splittings of the integral. It is because the integration variable q in Eq. (8) is not the same as q', the variable that corresponds to the n'th subband. This leads to the fact that the q width at the n'th subband band edge is much narrower than that for the $n = n'$ case. The q widths for the $n \neq n'$ and $n = n'$ cases are, respectively, of the order of η and $\sqrt{\eta}$. As such, the at-the-band-edge contribution to $I_{nn'}$ for $n \neq n'$ is negligible.

Returning to the I_{nn} terms, where $n \neq n_0$, we expect a severe cancellation between the at-the-band-edge and non-band-edge contributions. Analytical expressions for these two contributions will be obtained in the following, from which we can access their respective magnitudes directly. Splitting the I_{nn} terms accordingly, we have

$$I_{nn} = I^{(0)}_{nn} + I^{(\rm NBE)}_{nn} + I^{(\pi)}_{nn}, \tag{11}$$

where $I^{(0)}_{nn}$ and $I^{(\pi)}_{nn}$ are the at-the-band-edge integrals at band edges $q = 0$ and π, respectively. The band-edge energy at $q = 0$ $(q = \pi)$ is $\varepsilon_{n,\rm min}$ $(\varepsilon_{n,\rm max})$. Using Eq. (A9), we have

$$I^{(0)}_{nn} = -\frac{\pi\,\varepsilon_{n,\rm min}}{2\beta_n}\int_0^{\alpha} dq\,{\rm Re}\left[\frac{i}{\Delta} + L\right], \tag{12}$$

where $\Delta = \sqrt{q^2 - i\tilde{\eta}}$, $\tilde{\eta} = \varepsilon_{n,\rm min}\eta/\beta_n$, and $\beta_n = -\cos(k_{nx}a)$. The integration range is up to α, which is taken to be of the order of tens of $\sqrt{\tilde{\eta}}$. The expression is for the $\Delta L \ll 1$ case, with the L-depending term in the integrand coming from the expansion of $e^{-i\Delta L}$. This $\Delta L \ll 1$ condition is already sufficient to give us important insights for a reasonable range of L because Δ is sufficiently small. Performing the integration in Eq. (12), we have

$$I^{(0)}_{nn} = \frac{\pi\,\varepsilon_{n,\rm min}}{2\beta_n}\left[\frac{\pi}{4} - \alpha\,L\right]. \tag{13}$$

$I^{(\pi)}_{nn}$ can be shown to have the form similar to Eq. (12), except that $\varepsilon_{n,\rm min}$, $q^2 - i\tilde{\eta}$, and L are changed to $\varepsilon_{n,\rm max}$, $\tilde{q}^2 + i\tilde{\eta}$, and $-L$, respectively. Here, $\tilde{q} = \pi - q$, and

$$I^{(\pi)}_{nn} = -\frac{\pi\,\varepsilon_{n,\rm max}}{2\beta_n}\left[\frac{\pi}{4} - \alpha\,L\right]. \tag{14}$$

The non-band-edge integral is given by

$$I^{(\rm NBE)}_{nn} = -\frac{\pi}{4\beta_n}\int_{\alpha}^{\pi-\alpha} dq\,\frac{\sin(2qL)}{\sin q}\,\varepsilon_{\mathbf{k}_n}, \tag{15}$$

where Eq. (A8) has been used for $g^{12}_n(-\varepsilon_{\mathbf{k}_n})$. It is more convenient to express in terms of the integral that covers the entire q range, given by

$$I^{(\rm NBE)}_{nn} = -\frac{\pi}{4\beta_n}\int_0^{\pi} dq\,\frac{\sin(2qL)}{\sin q}\varepsilon_{\mathbf{k}_n} - \frac{\pi L\alpha[\varepsilon_{n,\rm max} - \varepsilon_{n,\rm min}]}{2\beta_n}. \tag{16}$$

Note that, in Eq. (16), the second (linear L) term cancels that in $I^{(0)}_{nn}$ and $I^{(\pi)}_{nn}$, given respectively by Eqs. (13) and (14). The integral in the first term in Eq. (16), apart from a factor $-\pi/(4\beta_n)$, is defined by

$$\mathfrak{I}_n = \int_0^{\pi} dq\,\frac{\sin(2qL)}{\sin q}\sqrt{1 + 4\beta_n^2 - 4\beta_n\cos q}, \tag{17}$$

where $\varepsilon_{\mathbf{k}_n} = \sqrt{1 + 4\beta_n^2 - 4\beta_n\cos q}$ can be evaluated (see Appendix B) to give

$$\mathfrak{I}_n = -\frac{\pi}{2}[\varepsilon_{n,\rm max} - \varepsilon_{n,\rm min}] + \pi\sqrt{1 + 4\beta_n^2} \times \sum_{k=L}^{\infty}\sum_{m=L}^{k}\frac{(4k)!\,b_n^{2k+1}}{(2k)!\,2^{6k+1}(k-m)!(k+m+1)!}, \tag{18}$$

where $b_n = 4\beta_n/(1 + 4\beta_n^2)$.

We point out that this is a remarkable result. First of all, if we substitute the first term in Eq. (18) to Eq. (16), and then sum up with Eqs. (13) and (14), we indeed see explicitly the exact cancellation, or the zero contribution to I_{nn} in Eq. (11). The residual contribution to I_{nn} hence comes from the second term in Eq. (18). The order of magnitude of this second term can be estimated by taking the $k = m = L$ term in Eq. (18) to give $(4L)!\,b_n^{2L+1}/[(2L)!\,2^{6L+1}(2L+1)!] \sim 2^{-2L-1.5}$, where we have taken $b_n \sim 1$, and the Stirling formula $n! \approx \sqrt{2\pi n}(n/e)^n$. This gives very small results for, say, $L > 5$. The same small order of magnitude also applies to cases of $n \neq n'$, according to the understanding we have drawn from Eq. (10). Second, the term in $I^{(\rm NBE)}_{nn}$ that participates in the cancellation, given by $\pi^2[\varepsilon_{n,\rm max} - \varepsilon_{n,\rm max}]/(8\beta_n)$, has a unity order of magnitude. Third, according to our derivation of $\mathfrak{I}_n$ in Eq. (18) (Appendix B), we see that the term participating in the cancellation is resulted from the integration over the entire q region. In contrast, the at-the-band-edge results in $I^{(0)}_{nn} + I^{(\pi)}_{nn}$ pick up their values only at the band-edge energies. This large difference in the range of energy, from which the at-the-band-edge and the non-band-edge cancellation terms accumulate their values, strongly hints that the cancellation terms could be affected differently should other effect, such as multiple scattering, be included. The subsequent disruption to the exact cancellation and the large change in the values of I_{nn} it might lead to now seems not as surprising as it would initially sound.

The calculation of $I_{n_0n_0}$ is carried out by substituting $\beta_{n_0} = \frac{1}{2}$ into Eqs. (11) and (16), with $\varepsilon_{n_0,\max} = 2$ and $\varepsilon_{n_0,\min} = 0$, to get

$$I_{n_0n_0} = -2\pi\left[\frac{1}{4}\int_0^{\pi} dq\,\frac{\sin(2qL)}{\cos(q/2)} + \frac{\pi}{4}\right]. \tag{19}$$

Inside the square brackets in Eq. (19), the first term equals $-\sum_{m=0}^{2L-1}\frac{(-1)^m}{2m+1}$ [43], the second term is reexpressed by the identity $\sum_{m=0}^{\infty}\frac{(-1)^m}{2m+1} = \pi/4$, and we have

$$I_{n_0n_0} = -2\pi\sum_{m=0}^{\infty}\frac{(-1)^m}{4L+(2m+1)}. \tag{20}$$

The summation over m in Eq. (20), apart from a factor -2π, can be further simplified, for $L > 5$, by assuming the summation to be proportional to L^{-1}, given by $\mathbb{C}/L$. We obtain from the explicit summation form in Eq. (20) the relation

$$\frac{1}{4L+1} - \frac{\mathbb{C}}{L+1/2} = \frac{\mathbb{C}}{L}, \tag{21}$$

from which we obtain

$$\mathbb{C} = \frac{L(2L+1)}{(4L+1)^2} \cong \frac{1}{8}. \tag{22}$$

In summary, we have

$$J_{\rm eff}^{(1)} = -\frac{4J^2}{\pi}\,\varphi_{n_0}^2(1,2)\sum_{m=0}^{\infty}\frac{(-1)^m}{4L+(2m+1)}$$
$$\cong -\frac{J^2}{2\pi\,L}\,\varphi_{n_0}^2(1,2) \quad \text{for } L > 5. \tag{23}$$

This analytic expression for $J_{\rm eff}^{(1)}$ has included only the I_{nn} term for $n = n_0$, the gapless subband of the metallic AGNR. That this expression is good for $L > 5$ has been discussed above, and is confirmed in Fig. 3, when the analytic $J_{\rm eff}^{(1)}$ results for AA-type (red triangles) and AB-type (red half-filled circles) magnetic-impurity pairs compare remarkably with the numerical $J_{\rm eff}^{(1)}$ results, given by black triangles and black half-filled circles, respectively. The numerical $J_{\rm eff}^{(1)}$ results are the direct evaluation of Eqs. (10) and (7). The L^{-1} dependence, the ferromagnetic coupling feature, and the order of magnitude of $J_{\rm eff}^{(1)}$ agree well with the $J_{\rm eff}$ calculation that made use of an effective (near zero-energy) Hamiltonian [30]. However, in this work, the full tight-binding Hamiltonian has been used. This nice correspondence manifests the fact that the gapless subband dominates the contribution to $J_{\rm eff}^{(1)}$. Note that $J_{\rm eff}^{(1)}$ has been multiplied by 10^2 in Fig. 3.

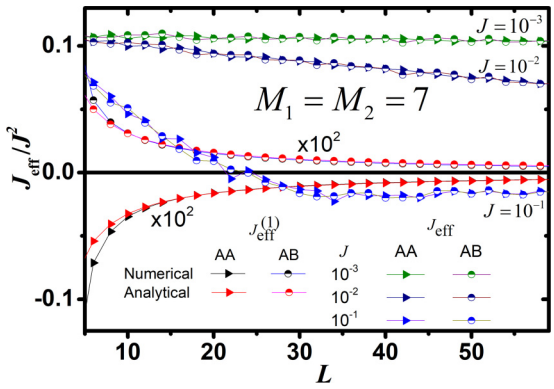

FIG. 3. Plot of $J_{\rm eff}/J^2$ versus L for three values of J. Both $J_{\rm eff}$ and J are in units of t_0. The AGNR ($W = 20$) has two magnetic impurities at $M_1 = M_2 = 7$, and a longitudinal separation L (in units of $\sqrt{3}a$). Both AA (triangles) and AB (half-filled circles) types are shown, for $J = 10^{-3}$ (green), 10^{-2} (dark blue), and 10^{-1} (light blue). Also shown are the LO-RKKY results $J_{\rm eff}^{(1)}/J^2$, amplified by 10^2, both numerical (black) and analytical (red).

The key result in this section, which we want to stress again here, is to turn our attention toward the gapped subbands. We establish, for incident electrons in an nth subband ($n \neq n_0$), the concept of severe cancellation between contributions to $J_{\rm eff}^{(1)}$ from the at-the-band-edge states and the non-band-edge states, and of the same order of magnitude these two cancellation terms are to the LO-RKKY coupling $J_{\rm eff}^{(1)}$.

B. Different-site type $J_{\rm eff}^{(1),\rm AB}$

In this section, we consider a different-site-type magnetic-impurity pair on AGNRs. For the sake of specificity for our discussion, we choose the $\mathcal{I} = 1$ ($\mathcal{I} = 2$) impurity to be located at the A (B) site. The different-site-type LO-RKKY coupling $J_{\rm eff}^{(1),\rm AB}$ is obtained from Eq. (6) when $C^{\rm A}(\gamma\varepsilon_{\mathbf{k}_n}) = 1/\sqrt{2}$ and $C^{\rm B}(\gamma\varepsilon_{\mathbf{k}_n}) = \overline{\gamma}h^*(\mathbf{k}_n)/(\sqrt{2}\varepsilon_{\mathbf{k}_n})$ is used, to give

$$J_{\rm eff}^{(1),\rm AB} = \frac{2J^2}{\pi^2}\sum_{n,n'}\varphi_n(1,2)\,\varphi_{n'}(1,2)\,I_{nn'}^{\rm AB},$$
$$I_{nn'}^{\rm AB} = \int_0^{\pi} dq\,{\rm Re}\big[g_{n',\rm AB}^{12}(-\varepsilon_{\mathbf{k}_n})\big]\,f_n^{\rm AB}(q), \tag{24}$$

where

$$f_n^{\rm AB}(q) = \frac{\big[\cos(qL) - 2\beta_n\cos(q|L_{12}-1|)\big]}{\varepsilon_{\mathbf{k}_n}}. \tag{25}$$

Here, $g_{n',\rm AB}^{12}(-\varepsilon_{\mathbf{k}_n})$ is given by Eq. (A2). For the sake of notation simplicity, no subscripts or superscripts will be used to indicate same-site-type physical parameters, whereas superscripts or subscripts (AB) will be used to indicate different-site-type physical parameters.

Again, as was discussed in the previous subsection, the form of Eq. (24) warrants the separation of the $I_{nn}^{\rm AB}$ into at-the-band-edge and non-band-edge terms for gapped nth subbands. That the sum of the two terms gives very small result can be easily seen from an alternate form of Eq. (24), in which $I_{nn'}^{\rm AB}$ is replaced by a new expression

$$I_{nn'}^{\rm AB} = \int_0^{\pi} dq\int_0^{\pi} dq'\,\frac{f_n^{\rm AB}(q)f_{n'}^{\rm AB}(q')}{\varepsilon_{\mathbf{k}_n} + \varepsilon_{\mathbf{k}'_{n'}}}. \tag{26}$$

The form of $I_{nn'}^{\rm AB}$ in Eq. (26) can be identified by substituting into Eq. (24) the expression of $g_{n',\rm AB}^{12}(-\varepsilon_{\mathbf{k}_n})$, and perform interchanging of the subband indices ($n \leftrightarrow n'$) and the integration variables ($q \leftrightarrow q'$) to the expression for $J_{\rm eff}^{(1),\rm AB}$ in Eq. (24). With this no-pole form in the integrand of $I_{nn'}^{\rm AB}$, the argument we had in the previous subsection applies here so that only the gapless subband ($n = n_0$) dominates the contribution to $J_{\rm eff}^{(1),\rm AB}$.

Note, however, that there is a sign difference between $I_{nn'}$ in Eq. (10) and $I_{nn'}^{\rm AB}$ in Eq. (26). This sign comes from the

$g^{12}_{n',\mathrm{AB}}(-\varepsilon_{\mathbf{k_n}})$ in Eq. (24), where its expansion consists of a summation over γ', allowing a factor $\overline{\gamma}'$ from the $C^{\mathrm{B}}(\mathbf{k}_n,\gamma')$ coefficient to come into play.

Performing the integral in Eq. (26) (see Appendix C) we get

$$J^{(1),\mathrm{AB}}_{\mathrm{eff}} = \frac{J^2}{2\pi(L+1/2)}\varphi^2_{n_0}(1,2), \tag{27}$$

for the case when impurity $\mathcal{I}=2$ has a larger longitudinal coordinate than the impurity $\mathcal{I}=1$, that is $L_{12}=-L$.

III. RKKY COUPLING: MULTIPLE SCATTERING

The numerical evaluation of J_{eff} is from obtaining $\langle V\rangle(S_1S_2)$ in Eq. (4), for the case when full multiple scattering is incorporated, and using the relation

$$J_{\mathrm{eff}} = \tfrac{1}{2}[\langle V\rangle(\uparrow\uparrow) - \langle V\rangle(\uparrow\downarrow)]. \tag{28}$$

To obtain for Eq. (4) the scattering wave function $\Psi_{\mathbf{k}_n,\nu,\nu}(\mathcal{I})$ at the site of the magnetic impurity, we use Eq. (3) to get

$$\begin{aligned}\Psi_{\mathbf{k}_n,\nu,\nu}(\mathcal{I}) = \psi_{\mathbf{k}_n}(\mathcal{I}) &+ \nu J\, G_{\mathcal{I}\mathcal{I}}(-\varepsilon_{\mathbf{k}_n})\Psi_{\mathbf{k}_n,\nu,\nu}(\mathcal{I})S_{\mathcal{I}}\\ &+\nu J\, G_{\mathcal{I}\overline{\mathcal{I}}}(-\varepsilon_{\mathbf{k}_n})\Psi_{\mathbf{k}_n,\nu,\nu}(\overline{\mathcal{I}})S_{\overline{\mathcal{I}}},\end{aligned} \tag{29}$$

where $\mathcal{I}\in 1,2$ denote a magnetic-impurity pair and $\overline{\mathcal{I}}$ refers to the partner of the magnetic impurity $\mathcal{I}$. Solving the set of equations in Eq. (29) gives

$$\Psi_{\mathbf{k}_n,\nu,\nu}(\mathcal{I}) = \frac{\psi_{\mathbf{k}_n}(\mathcal{I}) - \nu J S_{\overline{\mathcal{I}}}\big[G_{\overline{\mathcal{I}}\,\overline{\mathcal{I}}}\psi_{\mathbf{k}_n}(\mathcal{I}) - G_{\mathcal{I}\overline{\mathcal{I}}}\psi_{\mathbf{k}_n}(\overline{\mathcal{I}})\big]}{\mathcal{D}(-\varepsilon_{\mathbf{k}_n})}, \tag{30}$$

where

$$\begin{aligned}\mathcal{D}(-\varepsilon_{\mathbf{k}_n}) = 1 &- \nu J[\,G_{\mathcal{I}\mathcal{I}}S_{\mathcal{I}} + G_{\overline{\mathcal{I}}\,\overline{\mathcal{I}}}S_{\overline{\mathcal{I}}}\,]\\ &+ J^2 S_{\mathcal{I}}S_{\overline{\mathcal{I}}}[G_{\mathcal{I}\mathcal{I}}G_{\overline{\mathcal{I}}\,\overline{\mathcal{I}}} - G_{\mathcal{I}\overline{\mathcal{I}}}G_{\overline{\mathcal{I}}\mathcal{I}}].\end{aligned} \tag{31}$$

All the Green's functions in Eqs. (30) and (31) are functions of $-\varepsilon_{\mathbf{k}_n}$.

We show in the following that $\Psi_{\mathbf{k}_n,\nu,\nu}(\mathcal{I})$ is finite, or even zero, when $E=-\varepsilon_{\mathbf{k}_n}$ is at the nth subband band edge. To see this, we first note that within the square brackets in the numerator of Eq. (30), $G_{\overline{\mathcal{I}}\,\overline{\mathcal{I}}}\psi_{\mathbf{k}_n}(\mathcal{I}) - G_{\mathcal{I}\overline{\mathcal{I}}}\psi_{\mathbf{k}_n}(\overline{\mathcal{I}})$ no longer carries the singular nature of the Green's function at the nth subband band edge. This observation can be reached by substituting into Eq. (30) the at-the-band-edge behavior of the Green's function, given by Eq. (A11), and the expression for $\psi_{\mathbf{k}_n}$, given by Eq. (A4).

Turning to the denominator of Eq. (30), or Eq. (31), we can show similarly as in the previous paragraph that the coefficient of $J^2S_{\mathcal{I}}S_{\overline{\mathcal{I}}}$, given by $G_{\mathcal{I}\mathcal{I}}G_{\overline{\mathcal{I}}\,\overline{\mathcal{I}}} - G_{\mathcal{I}\overline{\mathcal{I}}}G_{\overline{\mathcal{I}}\mathcal{I}}$ exhibits cancellation that reduces its singular nature, from that of the square of a Green's function to that of a Green's function, at the nth subband band edge. The coefficient of the other term, which is proportional to νJ and given by $G_{\mathcal{I}\mathcal{I}}S_{\mathcal{I}} + G_{\overline{\mathcal{I}}\,\overline{\mathcal{I}}}S_{\overline{\mathcal{I}}}$, carries the singular nature of a Green's function at the nth subband band edge either when $S_{\mathcal{I}}=S_{\overline{\mathcal{I}}}$, or when $S_{\mathcal{I}}=-S_{\overline{\mathcal{I}}}$ and $M_1\neq M_2$. And we will have $\Psi_{\mathbf{k}_n,\nu,\nu}(\mathcal{I})=0$. However, for the case when $S_{\mathcal{I}}=-S_{\overline{\mathcal{I}}}$ and $M_1=M_2$, the term proportional to νJ becomes finite at the nth subband band edge. This will give rise to a zero $\Psi_{\mathbf{k}_n,\nu,\nu}(\mathcal{I})$, through the $J^2S_{\mathcal{I}}S_{\overline{\mathcal{I}}}$ term in the denominator, or to a finite $\Psi_{\mathbf{k}_n,\nu,\nu}(\mathcal{I})$, for cases of very small J. To sum up what we have discussed here, we see that $\Psi_{\mathbf{k}_n,\nu,\nu}(\mathcal{I})$, the total wave function corresponding to an incident state $|\psi_{\mathbf{k}_n}\rangle$ and at the sites of the magnetic impurities, are either zero or finite in all possible cases at the nth subband band edge. This is the result of multiple scatterings. More importantly, this has removed completely the at-the-band-edge contribution to J_{eff}. In other words, the numerical evaluation of $\langle V\rangle(S_1S_2)$, in Eq. (4), can be carried out by merely performing the k integral in the non-band-edge region only.

We present in Fig. 3 J_{eff}/J^2 versus L for $J=10^{-1}$ (light blue), 10^{-2} (dark blue), and 10^{-3} (green). Both AA- (triangles) and AB-type (half-filled circles) magnetic impurity pairs are shown. The transverse locations of the two magnetic impurities are at $M_1=M_2=7$ and the AGNR has $W=20$ carbon chains. Also shown are the LO-RKKY results, $J^{(1)}_{\mathrm{eff}}/J^2$ versus L, albeit multiplying a factor 10^2, where the numerical results (black), Eq. (10), and the analytical results (red), Eq. (23), are plotted for comparison.

First of all, it is clear that the $J^{(1)}_{\mathrm{eff}}$ results in Fig. 3 make their presence evident only after multiplying by a factor of 10^2. The correspondence between the numerical and the analytical results of $J^{(1)}_{\mathrm{eff}}$ has been remarkable for $L>5$. Decent correspondence is shown even in the $L\approx 5$ region. All these results firmly support the physical picture that we have developed in the LO-RKKY coupling, namely, that there is severe cancellation between contributions from the at-the-band-edge and non-band-edge states in gapped subbands, and that the dominant contribution is from the gapless subband. Furthermore, the AA-type (BB-type) magnetic-impurity pair exhibits ferromagnetic (antiferromagnetic) coupling.

The J_{eff} curves in Fig. 3 show drastically different physical characteristics from that of the $J^{(1)}_{\mathrm{eff}}$. Apart from the aforementioned much larger magnitude in J_{eff} than that in $J^{(1)}_{\mathrm{eff}}$, magnetic-impurity pairs of both sublattice site types exhibit similar characteristics in J_{eff}. This is to contrast with $J^{(1)}_{\mathrm{eff}}$, where coupling is ferromagnetic (antiferromagnetic) for the AA (AB) sublattice-site type. The J_{eff}'s for both sublattice-site types are antiferromagnetic for sufficiently low J and L. In the small-L region, the slopes of the J_{eff}/J^2 curves are more negative for larger J. It is interesting to see that J_{eff} can change from antiferromagnetic to ferromagnetic as L increases. As is shown in Fig. 3 by the $J=10^{-1}$ curve, J_{eff} changes sign at around $L=20$.

In Fig. 4 we present the J dependence of J_{eff}/J^2 for $L=14$, 28, and 42. System parameters are the same as those in Fig. 3. The RKKY coupling of both sublattice-site types exhibits similar characteristics, as we have obtained in the L dependence of J_{eff}. The slope of J_{eff}/J^2 versus J is more negative for larger L. For a given L, the coupling characteristics can change from antiferromagnetic to ferromagnetic when J increases. This is shown by the $L=42$ curve, where J_{eff} changes sign at around $J=005$.

Analytic expressions of J_{eff}

In this section, we derive analytic expressions for J_{eff} in the small-J ($J\ll 1$) regime, and for both the same-site and different-site type magnetic-impurity pairs. These analytic results allow us to compare with our full numerical results,

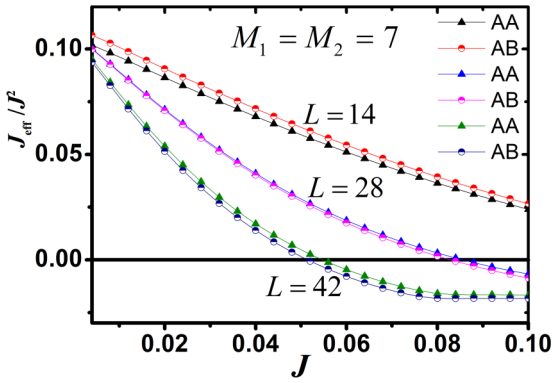

FIG. 4. Plot of $J_{\rm eff}/J^2$ versus J for three values of L. The AGNR ($W = 20$) has two magnetic impurities at $M_1 = M_2 = 7$. Both AA (triangles) and AB (half-filled circles) types are shown, for $L =$ 14, 28, and 42, in units of $\sqrt{3}a$.

and also to extract better physical understandings from our full numerical results. To make connection with the LO-RKKY results, it is more convenient to express the full wave function $\Psi_{\mathbf{k}_n\nu,\nu}(\mathcal{I})$ in the form

$$\Psi_{\mathbf{k}_n\nu,\nu}(\mathcal{I}) = \psi_{\mathbf{k}_n}(\mathcal{I}) + \Psi^{\rm SC}_{\mathbf{k}_n}(\mathcal{I}), \tag{32}$$

where the expression for $\Psi^{\rm SC}_{\mathbf{k}_n}(\mathcal{I})$ can be obtained from Eq. (30). The average $\langle V\rangle$, according to Eq. (4), hence takes on two terms

$$\langle V\rangle = U_1 + U_2, \tag{33}$$

where

$$U_1 = 2J\sum_{\mathcal{I}}\sum_{\mathbf{k}_n,\nu}{}' \,{\rm Re}\big[\,\psi^*_{\mathbf{k}_n}(\mathcal{I})\Psi^{\rm SC}_{\mathbf{k}_n}(\mathcal{I})\,\big]\nu S_{\mathcal{I}},$$
$$U_2 = J\sum_{\mathcal{I}}\sum_{\mathbf{k}_n,\nu}{}' \big|\Psi^{\rm SC}_{\mathbf{k}_n}(\mathcal{I})\big|^2\nu S_{\mathcal{I}}. \tag{34}$$

Here, the primed $\mathbf{k}_n$ summation denotes summing over the non-band-edge states only, as have been discussed above in this section.

Our goal is to extract from U_1 a term, denoted by U_{11}, akin to the LO-RKKY [given by Eq. (5)] expression but include only the non-band-edge incident states. Toward this end, the strategy is to remove the ν dependence in the denominator $\mathcal{D}(-\varepsilon_{\mathbf{k}_n})$ of $\Psi^{\rm SC}_{\mathbf{k}_n}(\mathcal{I})$ and perform the extraction to get

$$U_1 = U_{10} + U_{11} + U_{12}. \tag{35}$$

Here, U_{10} depends only on $S^2_{\mathcal{I}}$ and does not contribute to $J_{\rm eff}$. Expressions for the other two terms are given by

$$U_{11} = 8J^2S_1S_2\sum_{\mathbf{k}_n}{}' {\rm Re}[G_{12}]\,{\rm Re}\big[\psi^*_{\mathbf{k}_n}(1)\psi_{\mathbf{k}_n}(2)\big] \tag{36}$$

and

$$U_{12} = 4J^2\sum_{\mathbf{k}_n}{}' {\rm Re}\left[\frac{\zeta_{n1}(-\varepsilon_{\mathbf{k}_n}) + \zeta_{n2}(-\varepsilon_{\mathbf{k}_n})}{\mathfrak{D}(-\varepsilon_{\mathbf{k}_n})}\right], \tag{37}$$

where

$$\mathfrak{D} = 1 - J^2\sum_{\mathcal{I},\mathcal{I}'} G_{\mathcal{I}\mathcal{I}'}G_{\mathcal{I}'\mathcal{I}}S_{\mathcal{I}}S_{\mathcal{I}'} + J^4S_1^2S_2^2\Delta\mathcal{G}^2 \tag{38}$$

and

$$\zeta_{n1} = (1-\mathfrak{D})\sum_{\mathcal{I},\mathcal{I}'} S_{\mathcal{I}}S_{\mathcal{I}'}G_{\mathcal{I}\mathcal{I}'}\,{\rm Re}\big[\psi^*_{\mathbf{k}_n}(\mathcal{I})\psi_{\mathbf{k}_n}(\mathcal{I}')\big],$$
$$\zeta_{n2} = J^2\Delta\mathcal{G}S_1^2S_2^2\sum_{\mathcal{I},\mathcal{I}'}(-1)^{\delta_{\mathcal{I}\mathcal{I}'}}G_{\mathcal{I}\mathcal{I}'}\,{\rm Re}\big[\psi^*_{\mathbf{k}_n}(\overline{\mathcal{I}})\psi_{\mathbf{k}_n}(\overline{\mathcal{I}'})\big]. \tag{39}$$

Here, $\Delta\mathcal{G} = G_{11}G_{12} - G^2_{12}$ and $\delta_{\mathcal{I}\mathcal{I}'}$ is the Kronecker delta function. All the Green's functions in Eqs. (38) and (39) are functions of $-\varepsilon_{\mathbf{k}_n}$, which have been kept implicit for our presentation purposes.

The evaluation of U_{11} for the same-site type magnetic-impurity pairs is facilitated by identifying, from comparing Eqs. (36) and (5), that it is the non-band-edge term of the LO-RKKY results. Contributions from the $n \neq n_0$ subbands are obtained from Eqs. (16) and (18), whereas contribution from the n_0 subband is obtained from Eqs. (23) and (14). Putting these results together gives

$$U_{11} = J^2S_1S_2\left[-\frac{\varphi^2_{n_0}(1,2)}{2\pi L} + \sum_n \frac{\varphi^2_n(1,2)\Delta\varepsilon_n}{4\beta_n}\right], \tag{40}$$

where $\Delta\varepsilon_n = \varepsilon_{n,\max} - \varepsilon_{n,\min}$. It is important to note that the first term of Eq. (40), having a L^{-1} dependence, is of opposite sign to the second term, which is L independent. More importantly, the second term is much larger than the first term, and this causes the RKKY to change from ferromagnetic coupling in $J^{(1)}_{\rm eff}$ to the antiferromagnetic coupling in $J_{\rm eff}$, when full multiple scattering is implemented.

The evaluation of $U^{\rm AB}_{11}$, the U_{11} for the case of different-site-type magnetic-impurity pairs, is facilitated similarly by seeing that it is the LO-RKKY result, from comparing Eqs. (36) and (24), albeit keeping only the non-band-edge term. For gapped subbands, we use the fact $I^{\rm AB}_{nn} \approx 0$ to see that the non-band-edge term of Eq. (24) equals the minus of the at-the-band-edge terms. Another fact at the band edges, when $q = 0$ ($q = \pi$) or $E = E_{\rm BE} = -\varepsilon_{n,\min}$ ($E_{\rm BE} = -\varepsilon_{n,\max}$), that the reduced Green's functions of the different-site and the same-site types satisfy the relation

$$\big[g^{12}_{n,{\rm AB}}(E)f^{\rm AB}_n(q)\big]_{E=E_{\rm BE}} = \big[g^{12}_n(E)\cos(qL)\big]_{E=E_{\rm BE}}, \tag{41}$$

causes the at-the-band-edge terms of I_{nn} and $I^{\rm AB}_{nn}$ to be the same. Together, we see that the non-band edge I_{nn} equals that of $I^{\rm AB}_{nn}$ for gapped subband n. For the gapless subband, we calculate the non-band edge $I_{n_0n_0}$ directly. Derivation of Eq. (41) can be obtained at $q = 0$ (or $0 < q < \alpha$) by using the different-site- (same-site-) type reduced Green's function expression (A12) [Eq. (A6)]. Here, $z_< = z_-$ and $z_\pm = 1 \pm i\sqrt{q^2 - i\varepsilon_{n,\min}\,\eta/\beta_n}$, where $\sqrt{z}$ is taken to be in quadrants I and IV. Similarly, at $q = \pi$ (or $\pi - \alpha < q < \pi$), the reduced Green's function expression is obtained for $z_< = z_-$ and $z_\pm = -1 \pm i\sqrt{\tilde{q}^2 + i\varepsilon_{n,\min}\,\eta/\beta_n}$. Here, $q = \pi - \tilde{q}$. Drawing on all we have from the above, we obtain

$$U^{\rm AB}_{11} = J^2S_1S_2\left[\frac{\varphi^2_{n_0}(1,2)}{2\pi\left(L+\frac{1}{2}\right)} + \sum_n \frac{\varphi^2_n(1,2)\Delta\varepsilon_n}{4\beta_n}\right]. \tag{42}$$

It is clear that U_{11} and $U^{\rm AB}_{11}$ are very close to each other, with a relative small difference arising from the gapless subband,

namely, from the first term inside the square brackets of U_{11} and $U_{11}^{\rm AB}$.

For the derivation of the small-J behaviors of U_{12} and U_2 in the following, we consider the case $M_1 = M_2$. In this case, we have $G_{11} = G_{22}$. Furthermore, we drop the J^4 term in $\mathfrak{D}(-\varepsilon_{\mathbf{k}_n})$ of Eq. (38), and obtain the integral form of the same-site type U_{12}, given by

$$U_{12} = \frac{2J^4}{\pi}\sum_n \varphi_n(1,1)\int_\alpha^{\pi-\alpha} dq\,\mathrm{Re}\left[\frac{\left[(1+2S_1S_2)G_{11}^2+G_{12}^2\right]G_{12}\cos(qL)+G_{11}\left[(1+2S_1S_2)G_{12}^2+G_{11}^2\right]}{1-2J^2\left(G_{11}^2+S_1S_2G_{12}^2\right)}\right]. \tag{43}$$

The integral form of the same-site type U_2 is given by

$$U_2 = -\frac{4S_1S_2J^4}{\pi}\sum_n \varphi_n(1,1)\int_\alpha^{\pi-\alpha} dq\,\frac{\mathrm{Re}\left[-G_{11}^{*}G_{12}^2+S_1S_2\left(G_{11}^2-G_{12}^2\right)G_{12}^{*}\cos(qL)\right]}{|\,1-2J^2\left(G_{11}^2+S_1S_2G_{12}^2\right)\,|^2}. \tag{44}$$

To get a reasonable approximation scheme for both the U_{12} and U_2 above, we see first of all that the integrands contain third (second) power in the Green's function in the numerator (denominator), and these Green's functions are all functions of $-\varepsilon_{\mathbf{k}_n}$. Therefore, as the integration variable q approaches its band edges, the nth subband term in these Green's functions will increase in its magnitude, leading also to the magnitude increasing of the integrand. Therefore, it is reasonable to expect that significant contributions are from integration regions in the vicinity of band edges. This is supported by observing that all the terms in the numerators contain G_{12} and its higher power product, and thus are rapidly oscillating with argument qL and its harmonics. The oscillatory nature helps limiting the significant contribution to the vicinity of the band edges (with a q width of order of J). As for the G_{12} in the denominator, we convert the denominator into its magnitude square form and then take the $qL \ll 1$ approximation. We also comment that the integrand becomes finite again at $q = \alpha$ (or $q = \pi - \alpha$). This is resulted from taking only the real part of the integrand for the integral. Thus, our approximation scheme is to perform the integral in the vicinity of each subband band edge while replacing the Green's function by its nth subband term at the corresponding band edge, and taking $qL \ll 1$ in the denominator $\mathfrak{D}$ (J^4 term neglected) appropriately. After some lengthly calculation we obtain the same-site type $J_{\rm eff}$, defined by Eq. (28), to give

$$J_{\rm eff} = J^2\left[-\frac{\varphi_{n_0}^2(1,2)}{2\pi L}+\sum_n\frac{\varphi_n^2(1,2)\Delta\varepsilon_n}{4\beta_n}\right] - \frac{J}{16L}\sum_n\varphi_n(1,1)[\vartheta(\lambda_{n\pi})-\vartheta(\lambda_{n0})], \tag{45}$$

where

$$\vartheta(x) = 4x[7-e^{-6x}-3e^{-4x}-3e^{-2x}] + [-13x+10x(1+2x)e^{-4x}+3x(1+4x)e^{-8x}] + 4x[1-e^{-8x^2}+8x^2]-16x^2e^{-4x} \tag{46}$$

and

$$\lambda_{n0} = \frac{LJ\varphi_n(1,1)\,\varepsilon_{n,\min}}{4\beta_n}, \qquad \lambda_{n\pi} = \frac{LJ\varphi_n(1,1)\,\varepsilon_{n,\max}}{4\beta_n}. \tag{47}$$

Of the four terms in Eq. (46), the first two terms are associated with U_{12} for $S_1S_2 = 1$, the third term is associated with U_{12} for $S_1S_2 = -1$, and the fourth term is associated with U_2.

Taking the $x \ll 1$ limit, when $\vartheta(x) \approx 48x^2$, we have

$$J_{\rm eff} \approx J^2\left[-\frac{\varphi_{n_0}^2(1,2)}{2\pi L}+\sum_n\frac{\varphi_n^2(1,2)\Delta\varepsilon_n}{4\beta_n}\right] - \frac{3LJ^3}{2}\sum_n\frac{\varphi_n^3(1,1)}{\beta_n}. \tag{48}$$

Both Eqs. (45) and (48) are our key analytic results in this work, which are in the $LJ < 1$ and $LJ \ll 1$ regimes, respectively. Comparison of the full numerical same-site-type $J_{\rm eff}$ results with the analytic results in Eq. (45) is shown in Fig. 5. The matching of the two results in the small-J regime is remarkable, both in the values as well as the slopes. That the range of matching has a larger-q range for a smaller L is consistent with the $LJ \ll 1$ condition of the analytic result.

Of the two terms in Eq. (48), the second term (non-square-bracketed term) correctly gives the negative slope in the $J_{\rm eff}$ versus L behavior in the small-L region, as shown in Fig. 3. The same term also correctly gives the negative slope in the

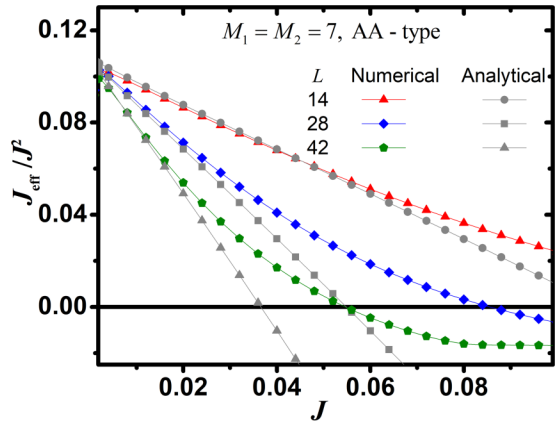

FIG. 5. Comparing full numerical results and small-J analytic results of $J_{\rm eff}/J^2$ versus J for three values of L. The AGNR ($W = 20$) has a same-site type magnetic-impurity pair at $M_1 = M_2 = 7$. Full numerical results for $L = 14$ (red), 28 (blue), and 42 (green) are shown. Analytic results for the corresponding L values are depicted by gray symbols.

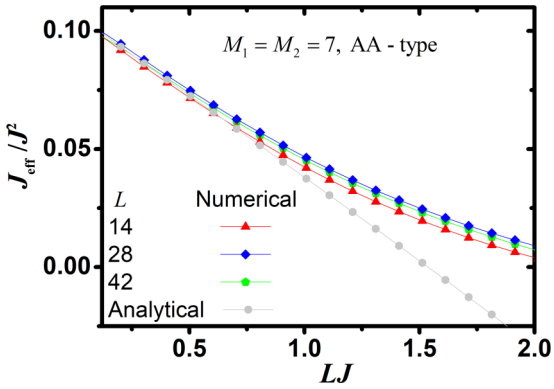

FIG. 6. Comparing the $J_{\rm eff}/J^2$ analytic results to the full numerical results in light of their dependence on LJ. The data are the same as in Fig. 5. The agreement shown is remarkable, with appreciable deviation occurring at $LJ \sim 1.0$ and greater values.

$J_{\rm eff}/J^2$ versus J behavior in the small-J region, as shown in Fig. 5. Finally, the role of LJ in the above comparison between the numerical and the analytical [Eq. (45)] results is presented in Fig. 6. The agreement shown is remarkable, in the $LJ < 1$ region, and with appreciable deviation occurs at $LJ \sim 1.0$ and greater values.

Derivation of the different-site-type RKKY couling, denoted by $J_{\rm eff}^{\rm AB}$, in the $LJ \ll 1$ regime, can be proceeded similarly to give

$$J_{\rm eff}^{\rm AB} \approx J^2\left[\frac{\varphi_{n_0}^2(1,2)}{2\pi\left(L+\frac{1}{2}\right)} + \sum_n \frac{\varphi_n^2(1,2)\Delta\varepsilon_n}{4\beta_n}\right] - \frac{3LJ^3}{2}\sum_n \frac{\varphi_n^3(1,1)}{\beta_n}. \quad (49)$$

The difference between the analytic expressions of $J_{\rm eff}$ and $J_{\rm eff}^{\rm AB}$ is in the contribution from the n_0th subband, that is, the first term inside the square-bracketed term. This difference leads only to a very small relative deviation, and is consistent with our full numerical results for $J_{\rm eff}$ and $J_{\rm eff}^{\rm AB}$, as is shown in Fig. 4.

IV. CONCLUSION

In conclusion, we have described the RKKY coupling $J_{\rm eff}$ for a magnetic-impurity pair on metallic AGNRs with multiple scattering of the mediating electrons fully implemented. We have derived an analytic expression for $J_{\rm eff}$ in the $LJ < 1$ regime. The remarkable matching of this analytic expression to that of the full numerical results confirms us the physical picture that significant gapped subband contributions to $J_{\rm eff}$ are from incident states in the non-band-edge region that is in the vicinity of the subband band edges. Thus, all the subbands, including the gapless and the gapped subbands, are contributing to $J_{\rm eff}$, and are roughly speaking on the same weighting. Key results obtained are that $J_{\rm eff}$ is found to be much larger than the Born approximation results, the LO-RKKY coupling $J_{\rm eff}^{(1)}$ results, by up to two orders of magnitude, and that the RKKY coupling is insensitive to the sublattice-site type of the magnetic-impurity pairs. Furthermore, $J_{\rm eff}$ is found to exhibit an antiferromagnetic to ferromagnetic coupling transition when L is increasing for a given J, or when J is increasing for a given L.

The above insights are closely tied to detail analysis we have performed for the subband contributions to the LO-RKKY coupling $J_{\rm eff}^{(1)}$. Analytic expressions are obtained for contributions from the gapless subband and, separately, from the at-the-band-edge and non-band-edge terms of a gapped subband. Severe cancellation between the at-the-band-edge and non-band-edge terms of a gapped subband is demonstrated analytically, leading to the fact that the gapless subband is the sole contributor to $J_{\rm eff}^{(1)}$. This explains why that the $J_{\rm eff}^{(1)}$ expression in this work agrees basically with the $J_{\rm eff}^{(1)}$ calculated from a near-zero-energy effective Hamiltonian [30], and on three shared features. The shared features of $J_{\rm eff}^{(1)}$ are the order of magnitude, the L^{-1} dependence, and the coupling characteristics: ferromagnetic (antiferromagnetic) for the same-site- (different-site-) type magnetic-impurity pairs. Yet, our key result is to bring our attention to the gapped subbands, by showing that the at-the-band-edge terms are each of the same order of magnitude as the $J_{\rm eff}^{(1)}$, and that the at-the-band-edge term is suppressed when full multiple scattering is implemented, thus opening up large contributions from gapped subbands to the RKKY coupling.

The dramatic enhancement in RKKY due to multiple scattering found in this work hinges on the fact that the density of states is singular at subband band edges. Quasi-one-dimensional systems such as AGNRs, carbon nanotubes, bilayer graphene nanoribbons, and nanoribbons form from novel two-dimensional systems all fall into this category. Thus, it is of great interest to explore the manifestation of our RKKY features in these candidate systems. Furthermore, recent study on Bernal bilayer graphene system has found logarithmic-singularity feature in the real-space propagator that involves sites in the bilayer that are on top of each other [27]. It would be of interest also to explore this system for the multiple scattering effects on the RKKY coupling.

We would like to comment on the possible experimental way to observe our large RKKY coupling results. Recent observation of π magnetism of a single carbon vacancy on graphene using scanning tunneling spectroscopy (STS) [44] is an exciting development. The measurement of the spin-split density of states in the nearest and next-nearest sites from the vacancy is a direct measure of the π magnetism of the single carbon vacancy. This novel technology could be further developed to probe the spin-split density of states in the vicinity sites of the two magnetic impurities for the study of the nature of the coupling, be it antiferromagnetic or ferromagnetic.

ACKNOWLEDGMENT

This work was supported by Taiwan Grant No. MOST 107-2112-M-009-009, and a MOE-ATU grant.

APPENDIX A: AGNR GREEN'S FUNCTION

The analytical expression of the AGNR Green's function $G_{\mathcal{J}\mathcal{J}'}(E)$ facilitates both the illustration of the key physics in this work and the efficiency in our numerical calculation. Thus, we opt, for completeness, to highlight some $G_{\mathcal{J}\mathcal{J}'}(E)$

expressions in the following, even though $G_{\mathcal{J}\mathcal{J}'}(E)$ had been obtained previously by one of the authors and his collaborator [45]. In addition, we present the $G_{\mathcal{J}\mathcal{J}'}(E)$ expression in the *at-the-bandedge* regime, a regime that had not been discussed previously [45], which corresponds to E aligning right at an AGNR subband band edge.

Starting with $G_{\mathcal{J}\mathcal{J}'}(E) = \langle\mathcal{J}|[E - H + i\eta]^{-1}|\mathcal{J}'\rangle$, for H described by the AGNR tight-binding Hamiltonian and $\mathcal{J} = (j, s) = (\mathbf{R}_j, s)$, the lattice-site coordinate depicted by the unit-cell position $\mathbf{R}_j$ and the site-type index s (A/B type), we have

$$G_{\mathcal{J}\mathcal{J}'}(E) = \frac{1}{2\pi}\sum_n \varphi_n(j, j')\, g_n^{\mathcal{J}\mathcal{J}'}(E), \tag{A1}$$

and the nth subband reduced Green's function $g_n^{\mathcal{J}\mathcal{J}'}(E)$ is given by

$$g_n^{\mathcal{J}\mathcal{J}'}(E) = \int_{-\pi}^{\pi} dq \sum_\gamma \frac{e^{iqL_{jj'}}\, C^s(\mathbf{k}_n,\, \gamma)\, C^{s'*}(\mathbf{k}_n,\, \gamma)}{E - \gamma\, \varepsilon(\mathbf{k}_n) + i\eta}. \tag{A2}$$

Here, n denotes the subband index and $\varphi_n(j, j')$ is associated with the nth subband amplitudes at the two lattice sites $\mathcal{J}$ and $\mathcal{J}'$, given by

$$\varphi_n(j, j') = \frac{4}{W+1}\sin\left[\frac{n\pi(M_j+1)}{W+1}\right]\sin\left[\frac{n\pi(M_{j'}+1)}{W+1}\right]. \tag{A3}$$

The wave vector $\mathbf{k}_n = (k_{nx}, k)$ where $k_{nx}a = n\pi/(W+1)$, and W denotes the width of the AGNR formed from W carbon chains with an interchain spacing $a = 1.23$ Å such that the unit-cell position $\mathbf{R}_j = M_j a\hat{x} + N_j\sqrt{3}a\hat{y}$. Across the width of the AGNR, the coordinate $0 \leqslant M \leqslant W - 1$. A metallic AGNR has $W = 3p + 2$ for integer p. The subband index n is chosen to take on values $W/2 + 1 \leqslant n \leqslant W$, for even W, so that k in a subband spans a fuller range, namely, $|k\sqrt{3}a| \leqslant \pi$.

In Eq. (A2), η is an infinitesimal positive quantity, γ denotes the sign of the subband energy $E(\mathbf{k}_n, \gamma) = \gamma\varepsilon(\mathbf{k}_n) = \gamma|h(\mathbf{k}_n)|$, where $h(\mathbf{k}_n) = 1 + 2\cos(k_{nx}a)\, e^{-iq}$ and $q = k\sqrt{3}a$. All energies are in units of $t_0 = 2.66$ eV, the hopping constant of graphene. In addition, $L_{jj'} = N_j - N_{j'}$, pseudospin coefficients $C^{\mathrm{A}}(\mathbf{k}_n, \gamma) = 1/\sqrt{2}$ and $C^{\mathrm{B}}(\mathbf{k}_n, \gamma) = \overline{\gamma}\, h^*(\mathbf{k}_n)/(\sqrt{2}\,\varepsilon(\mathbf{k}_n))$, and $\overline{\gamma} = -\gamma$. The wave function $\langle\mathcal{J}|\psi_{\mathbf{k}_n}\rangle$ for an AGNR subband state is given by

$$\langle\mathcal{J}|\psi_{\mathbf{k}_n}\rangle = \frac{2\, e^{iqN_j}\sin\left[\frac{n\pi(M_j+1)}{W+1}\right]}{\sqrt{(W+1)N_y}}\begin{pmatrix} C^{\mathrm{A}}(\mathbf{k}_n, \gamma) \\ \\ C^{\mathrm{B}}(\mathbf{k}_n, \gamma)\end{pmatrix}, \tag{A4}$$

where N_y are the total unit cells along $\hat{y}$ in the system (N_y is even for an AGNR), and γ is kept implicit in $|\psi_{\mathbf{k}_n}\rangle$ for notation simplicity.

The AGNR Green's function, as given by Eqs. (A1) and (A2), has the nice symmetry property

$$G_{\mathcal{J}\mathcal{J}'}(E) = G_{\mathcal{J}'\mathcal{J}}(E) \tag{A5}$$

for both the same-site ($ss' = $ AA or BB) type or different-site ($ss' = $ AB or BA) type. Equation (A5) can be obtained by changing, in Eq. (A2), the integration variable $q \to -q$ while making use of the fact that $\varepsilon(\mathbf{k}_n)$ and $C^{\mathrm{A}}(\mathbf{k}_n, \gamma)$ remain the same but $C^{\mathrm{B}}(\mathbf{k}_n, \gamma) \to C^{\mathrm{B}*}(\mathbf{k}_n, \gamma)$.

The same-site-type nth subband reduced Green's function $g_n^{\mathcal{J}\mathcal{J}'}(E)$ is found to be

$$g_n^{\mathcal{J}\mathcal{J}'}(E) = \frac{\pi E\, z_<^{|L_{jj'}|}}{\beta_n(z_< - z_>)}, \tag{A6}$$

where $z_<$ ($z_>$) refers to one of $z_\pm$ that has its magnitude less (greater) than unity. Expressed in terms of $z = e^{iq}$ to the equation $(E + i\eta)^2 - \varepsilon(\mathbf{k}_n)^2 = 0$, its roots denoted by $z_\pm$ are given by

$$z_\pm = \left(\cos Q - \frac{2iE\eta}{4\beta_n}\right) \pm \sqrt{\left(\cos Q - \frac{2iE\eta}{4\beta_n}\right)^2 - 1}. \tag{A7}$$

Here, Q is a dimensionless longitudinal wave vector, representing E via the relation $E^2 = 1 + 4\beta_n^2 - 4\beta_n\cos Q$, wherein $\beta_n = -\cos(k_{nx}a)$ is positive. The band-edge energies of the nth subband are given by $\varepsilon_{n,\min} = |1 - 2\beta_n|$ at $Q = 0$, and $\varepsilon_{n,\max} = 1 + 2\beta_n$ at $Q = \pi$. Q becomes complex when $|E| < \varepsilon_{n,\min}$ (or $|E| > \varepsilon_{n,\max}$), given by $Q = iQ_{\mathrm{I}}$ (or $Q = \pi + iQ_{\mathrm{I}}$). The form given in Eqs. (A6) and (A7) is sufficient for numerical evaluations of $g_n^{\mathcal{J}\mathcal{J}'}(E)$ for any E.

Two regimes, namely, the at-the-band-edge and the non-band-edge regimes, are of interest in this work. Equally importantly, the use of these two regimes are crucial when we want to perform analytical analysis. They are defined according to the values of E (or Q) with respect to the subband band edges. The at-the-band-edge regime is when E aligns right at a band edge, or more precisely, Q falls within a Q interval, centered at either $Q = 0$ or π, with an interval width of order $\sqrt{\eta}$. The non-band-edge regime is when Q does not fall within the at-the-band-edge interval. Should analytical analysis be needed, simplification of Eq. (A7) will be undertaken differently depending on which regimes we are working on at hand.

In the non-band-edge regime, Eq. (A7) can be simplified by expanding out the square-root term, up to first order in η. By this we have taken η to be the smallest energy scale. This gives us, for the case of the nth subband reduced Green's function and for real Q (or $\varepsilon_{n,\min} < |E| < \varepsilon_{n,\max}$), the expression

$$g_n^{\mathcal{J}\mathcal{J}'}(E) = \mp\frac{i\pi E}{2\beta_n}\frac{e^{\pm iQL}}{\sin Q}, \tag{A8}$$

where the upper (lower) sign corresponds to positive (negative) E, and $L = |L_{jj'}|$. Note that the factor $e^{\pm iQL}$ in Eq. (A8) gives the expected form of an outgoing wave. Furthermore, Eq. (A8) clearly shows that $g_n^{\mathcal{J}\mathcal{J}'}(E)$ grows in magnitude as Q approaches a band edge. A summation of, say, $g_n^{\mathcal{J}\mathcal{J}'}(E)$, over all incident energy E, or more appropriately over Q, leads to an integral of the form $\int dQ\, g_n^{\mathcal{J}\mathcal{J}'}(E)$, which might appear to be diverging had we allowed the integration to go all the way to the band edge. A correct way of performing the Q integral, however, is to separate it into two integration regions: the non-band-edge and the at-the-band-edge regions, with the two regions separated by a Q of order equal to tens of $\sqrt{\eta}$.

In the at-the-band-edge regime, we do not expand out the square-root term in Eq. (A7) but, rather, expand about Q with the form $Q = \tilde{Q}$ (at $\varepsilon_{n,\min}$) or $Q = \pi - \tilde{Q}$ (at $\varepsilon_{n,\max}$). Here, $\tilde{Q}$ represents a small deviation. This gives us the at-the-band-edge $g_n^{\mathcal{J}\mathcal{J}'}(E)$ expression, for E within the subband energy

and at $\varepsilon_{n,\min}$,

$$g_n^{\mathcal{J}\mathcal{J}'}(E) = \mp \frac{i\pi E}{2\beta_n} \frac{e^{\pm i\sqrt{\tilde{Q}^2 + iE\eta/\beta_n}\,L}}{\sqrt{\tilde{Q}^2 + iE\eta/\beta_n}}, \tag{A9}$$

and at $\varepsilon_{n,\max}$,

$$g_n^{\mathcal{J}\mathcal{J}'}(E) = \mp(-1)^L \frac{i\pi E}{2\beta_n} \frac{e^{\mp i\sqrt{\tilde{Q}^2 - iE\eta/\beta_n}\,L}}{\sqrt{\tilde{Q}^2 - iE\eta/\beta_n}}, \tag{A10}$$

where, again, the upper (lower) sign corresponds to positive (negative) E.

Equations (A9) and (A10) show that, as far as the η dependence is concerned, the Q (or $\tilde{Q}$) width is of order $\sqrt{\eta}$ and the $g_n^{\mathcal{J}\mathcal{J}'}(E)$ is not diverging, but has large values of the order of $1/\sqrt{\eta}$. Hence, the aforementioned Q integral in this at-the-band-edge region becomes finite, and is independent of η. It is important to note that when E is in the at-the-band-edge regime of the nth subband, $G_{\mathcal{J}\mathcal{J}'}(E)$ is dominated by the contribution from the nth subband. Taking, for instance, the same-site-type case when $E = \varepsilon_{n,\min}$, and $\mathcal{J} \neq \mathcal{J}'$, we have, from Eqs. (A1) and (A9),

$$G_{\mathcal{J}\mathcal{J}'}(\varepsilon_{n,\min}) \simeq \varphi_n(j, j')\, G_n(\varepsilon_{n,\min}) + \Delta G(n, j, j', L), \tag{A11}$$

where the first term is the dominating term with $G_n(E) = \mp i\sqrt{E}/[\,4\sqrt{i\beta_n\eta}\,]$, and the second term $\Delta G(n, j, j', L)$ is the collection of all remaining terms, including the summation of $n' \neq n$ subbands in Eq. (A1) and the expansion of the exponential factor in Eq. (A9). Similar form can be identified for $E = \varepsilon_{n,\max}$. Finally, the form in Eq. (A11) will be used in this work for the tracing of the dominating term.

The ifferent-site-type nth subband reduced Green's function $g_n^{\mathcal{J}\mathcal{J}'}(E)$ (for $ss' = \mathrm{BA}$), now adopted an explicit indexing notation $g_{n,\mathrm{BA}}^{jj'}(E)$, is found to be

$$g_{n,\mathrm{BA}}^{jj'}(E) = -\frac{\pi\, z_<^{|L_{jj'}|}}{\beta_n(z_< - z_>)} + \frac{2\pi\, z_<^{|L_{jj'}+1|}}{(z_< - z_>)}. \tag{A12}$$

The case of $g_{n,\mathrm{AB}}^{jj'}(E)$ can be obtained from Eq. (A12) by changing the exponent $|L_{jj'} + 1|$ in the second term to $|L_{jj'} - 1|$. The expressions of $g_{n,\mathrm{BA}}^{jj'}(E)$ in the at-the-band-edge and the non-band-edge regimes, not shown here, could be obtained similarly as have been illustrated above for the same-site-type case.

APPENDIX B: EVALUATION OF $\mathfrak{I}_n$

Evaluation of Eq. (17) is facilitated by adding the same integral $\mathfrak{I}_n$, but with a change in the integration variable $q = \pi - q'$, to give

$$\mathfrak{I}_n = \frac{\sqrt{1+4\beta_n^2}}{2} \int_0^\pi [\sqrt{1 - b_n \cos q} - \sqrt{1 + b_n \cos q}] \times \frac{\sin(2qL)}{\sin q}\, dq, \tag{B1}$$

where $b_n = 4\beta_n/(1 + 4\beta_n^2)$. Making use of the identity

$$\sqrt{1-x} - \sqrt{1+x} = -\sum_{k=0}^{\infty} \frac{x^{2k+1}}{(2k+1)!(2k)!} \frac{(4k)!}{2^{4k}}, \tag{B2}$$

and the result

$$\int_0^\pi \cos^{2k+1} q \frac{\sin(2qL)}{\sin q} dq = \frac{\pi}{2^{2k+1}} \sum_{j=0}^{L+\mathcal{N}} \frac{(2k+1)!}{(L+k-j)!} \times \frac{1}{(k+1-L+j)!}, \tag{B3}$$

where $\mathcal{N} = k$ if $0 \leqslant k \leqslant L-1$ and $\mathcal{N} = L-1$ if $L \leqslant k$, we get

$$\mathfrak{I}_n = -\frac{\pi\sqrt{1+4\beta_n^2}}{2} \left[\sum_{k=0}^{L-1} \sum_{m=-(k+1)}^{k} + \sum_{k=L}^{\infty} \sum_{m=-L}^{L-1} \right] \times \frac{(4k)!\, b_n^{2k+1}}{(2k)!2^{6k+1}(k-m)!(k+m+1)!}. \tag{B4}$$

In the first term in Eq. (B4), we replace the finite-k summation by an infinite-k summation plus a compensating term. The infinite-k summation term is called $\mathfrak{I}_{n1}$, while the sum of the compensating term and the second term in Eq. (B4) is called $\mathfrak{I}_{n2}$. As such, $\mathfrak{I}_n = \mathfrak{I}_{n1} + \mathfrak{I}_{n2}$, where

$$\mathfrak{I}_{n1} = -\frac{\pi\sqrt{1+4\beta_n^2}}{2} \sum_{k=0}^{\infty} \frac{(4k)!\, b_n^{2k+1}}{(2k)!2^{4k}(2k+1)!}. \tag{B5}$$

$\mathfrak{I}_{n1}$ can be further simplified, using Eq. (B2), to the form

$$\mathfrak{I}_{n1} = \frac{\pi\sqrt{1+4\beta_n^2}}{2} [\sqrt{1+b_n} - \sqrt{1-b_n}] = -\frac{\pi[\varepsilon_{n,\max} - \varepsilon_{n,\min}]}{2}. \tag{B6}$$

$\mathfrak{I}_{n2}$ can be simplified, by noticing that the terms for m and $-m-1$ in the m summation are the same, and can be shown equal to the second term in Eq. (18).

APPENDIX C: EVALUATION OF $I_{n_0 n_0}^{\mathrm{AB}}$

The method of evaluation of the integral $I_{n_0 n_0}^{\mathrm{AB}}$ could follow what we have used in Sec. II A for $I_{n_0 n_0}$, which result is given in Eq. (23). Here, however, we outline an alternate method of evaluation that starts from the no-pole form in Eq. (26). This alternate evaluation can be shown to produce the same result, in Eq. (23), for the case of the LO-RKKY coupling $J_{\mathrm{eff}}^{(1)}$ in the $L > 5$ region. The method is based on the expectation, according to the form of Eq. (26), that the most significant contribution to $I_{n_0 n_0}^{\mathrm{AB}}$ comes from the linear dispersion relation region (small-q region) of the gapless subband $n = n_0$, while larger-q region dies out rapidly due to the L-dependent oscillations.

For $n = n_0$ we have $\beta_{n_0} = \frac{1}{2}$ such that $f_{n_0}^{\mathrm{AB}}(q) = \{\cos(qL) - \cos[q(L+1)]\}/q \approx \sin[q(L+1/2)]$, and $\varepsilon_{\mathbf{k}_{n_0}} \approx q$. Here, we have used the $q \ll 1$ and $L_{12} = -L$

conditions. The equation for $I^{\mathrm{AB}}_{n_0 n_0}$ becomes

$$\begin{aligned} I^{\mathrm{AB}}_{\mathrm{n_0 n_0}} &\cong \int_0^\infty dq \int_0^\infty dq' \, \frac{\sin[q(L+1/2)]\sin[q'(L+1/2)]}{q+q'} \\ &= \int_0^\infty dq \int_0^\infty dq' \sin[q(L+1/2)]\sin[q'(L+1/2)] \int_0^\infty e^{-(q+q')\tau} d\tau \\ &= \frac{\pi}{4(L+1/2)}. \end{aligned} \tag{C1}$$

[1] M. A. Ruderman and C. Kittel, Phys. Rev. **96**, 99 (1954).
[2] T. Kasuya, Prog. Theor. Phys. **16**, 45 (1956).
[3] K. Yosida, Phys. Rev. **106**, 893 (1957).
[4] J. Geldenhuys and D. H. Wiid, J. Phys. F: Met. Phys. **8**, 2021 (1978).
[5] N. T. M. Hoa, E. Minamitani, W. A. Diño, B. T. Cong, and H. Kasai, J. Phys. Soc. Jpn. **79**, 074702 (2010).
[6] J. d'Albuquerque e Castro, M. S. Ferreira, and R. B. Muniz, Phys. Rev. B **49**, 16062 (1994).
[7] R. Bouzerar, G. Bouzerar, and T. Ziman, Phys. Rev. B **73**, 024411 (2006).
[8] H. Imamura, P. Bruno, and Y. Utsumi, Phys. Rev. B **69**, 121303(R) (2004).
[9] A. T. Costa Jr., D. F. Kirwan, and M. S. Ferreira, Phys. Rev. B **72**, 085402 (2005).
[10] K. S. Novoselov, A. K. Geim, S. V. Morozov, D. Jiang, Y. Zhang, S. V. Dubonos, I. V. Grigorieva, and A. A. Firsov, Science **306**, 666 (2004).
[11] K. S. Novoselov, D. Jiang, F. Schedin, T. J. Booth, V. V. Khotkevich, S. V. Morozov, and A. K. Geim, Proc. Natl. Acad. Sci. U. S. A. **102**, 10451 (2005).
[12] V. K. Dugaev, V. I. Litvinov, and J. Barnas, Phys. Rev. B **74**, 224438 (2006).
[13] S. Saremi, Phys. Rev. B **76**, 184430 (2007).
[14] J. E. Bunder and H. H. Lin, Phys. Rev. B **80**, 153414 (2009).
[15] P. Venezuela, R. B. Muniz, A. T. Costa, D. M. Edwards, S. R. Power, and M. S. Ferreira, Phys. Rev. B **80**, 241413(R) (2009).
[16] A. M. Black-Schaffer, Phys. Rev. B **81**, 205416 (2010).
[17] M. Sherafati and S. Satpathy, Phys. Rev. B **83**, 165425 (2011).
[18] M. Sherafati and S. Satpathy, Phys. Rev. B **84**, 125416 (2011).
[19] E. Kogan, Phys. Rev. B **84**, 115119 (2011).
[20] H. Lee, J. Kim, E. R. Mucciolo, G. Bouzerar, and S. Kettemann, Phys. Rev. B **85**, 075420 (2012).
[21] H. Lee, E. R. Mucciolo, G. Bouzerar, and S. Kettemann, Phys. Rev. B **86**, 205427 (2012).
[22] S. R. Power and M. S. Ferreira, Crystal **3**, 49 (2013).
[23] S. LeBohec, J. Talbot, and E. G. Mishchenko, Phys. Rev. B **89**, 045433 (2014).
[24] I. V. Krainov, I. V. Rozhansky, N. S. Averkiev, and E. Lahderanta, Phys. Rev. B **92**, 155432 (2015).
[25] M. Agarwal and E. G. Mishchenko, Phys. Rev. B **95**, 075411 (2017).
[26] Z. Shi, E. M. Nica, and I. Affleck, Phys. Rev. B **100**, 125158 (2019).
[27] N. Klier, S. Shallcross, and O. Pankratov, Phys. Rev. B **90**, 245118 (2014).
[28] N. Klier, S. Shallcross, S. Sharma, and O. Pankratov, Phys. Rev. B **92**, 205414 (2015).
[29] N. Klier, S. Sharma, O. Pankratov, and S. Shallcross, Phys. Rev. B **94**, 205436 (2016).
[30] J. Klinovaja and D. Loss, Phys. Rev. B **87**, 045422 (2013).
[31] K. Szalowski, J. Phys.: Condens. Matter **25**, 166001 (2013).
[32] K. Szalowski, Phys. Rev. B **90**, 085410 (2014).
[33] H. Rezania and F. Azizi, J. Magn. Magn. Mater. **417**, 272 (2016).
[34] F. S. M. Guimarães, J. Duffy, A. T. Costa, R. B. Muniz, and M. S. Ferreira, Phys. Rev. B **94**, 235439 (2016).
[35] B. D. Hoi and M. Yarmohammadi, J. Magn. Magn. Mater. **454**, 362 (2018).
[36] F. Parhizgar, H. Rostami, and R. Asgari, Phys. Rev. B **87**, 125401 (2013).
[37] M. Zare, F. Parhizgar, and R. Asgari, Phys. Rev. B **94**, 045443 (2016).
[38] O. Avalos-Ovando, D. Mastrogiuseppe, and S. E. Ulloa, Phys. Rev. B **99**, 035107 (2019).
[39] V. Kaladzhyan, A. A. Zyuzin, and P. Simon, Phys. Rev. B **99**, 165302 (2019).
[40] J. M. Duffy, P. D. Gorman, S. R. Power, and M. S. Ferreira, J. Phys.: Condens. Matter **26**, 055007 (2014).
[41] C. S. Chu and R. S. Sorbello, Phys. Rev. B **40**, 5941 (1989).
[42] P. F. Bagwell, Phys. Rev. B **41**, 10354 (1990).
[43] I. S. Gradshteyn and I. M. Ryzhik, *Table of Integrals, Series, and Products* (Academic, New York, 1980).
[44] Y. Zhang, S. Y. Li, H. Huang, W. T. Li, J. B. Qiao, W. X. Wang, L. J. Yin, K. K. Bai, W. Duan, and L. He, Phys. Rev. Lett. **117**, 166801 (2016).
[45] C. H. Chiu and C. S. Chu, Phys. Rev. B **90**, 195436 (2014).